

# Optical absorption and second harmonic generation in SiO<sub>2</sub>:DR1 sol-gel films as function of poling time.

Alfredo Franco<sup>a</sup>, Guadalupe Valverde-Aguilar<sup>b</sup>, Jorge García-Macedo<sup>\*a</sup>

<sup>a</sup>Instituto de Física, UNAM, P.O. Box 20-364, 01000 México, D.F., Mexico. E-mail: [gamaj@fisica.unam.mx](mailto:gamaj@fisica.unam.mx); phone (55) 56 22 51 03; fax (55) 56 22 51 11.

<sup>b</sup>Facultad de Ciencias, UNAM. Circuito exterior, CU. México, D.F. 04510

## ABSTRACT

Amorphous and nanostructured SiO<sub>2</sub>:DR1 sol-gel films were prepared by dip-coating. X-ray diffraction studies were performed to determine the long-order structure obtained in the films. The optical absorption (AO) measurements were done in three different nanostructures of the SiO<sub>2</sub> network: lamellar, hexagonal and mixed. The AO measurements and the second harmonic generation (SHG) intensity were carried out at different orientation steps of the chromophores embedded in the films. These chromophore orientation distributions were obtained by means of the corona technique, and they depend on the corona poling time. We physically model the optical absorption and the second harmonic generation experimental results as function of the corona poling time, employing only one fitting parameter related to the matrix-chromophore interactions. The physical model and the experimental results were in an excellent agreement. The experimental results fitted by the model are shown in plots of order parameter against corona poling time and SHG intensity against corona poling time. The lamellar structure provides a larger order parameter values than those obtained for the other structures. A minimum value for the order parameter was detected by means of the optical absorption measurements at short poling times. For the SHG measurements, four different chromophore concentrations were used. As the concentration increases the measured SHG intensity increases too, but the increment is limited by the electrostatic interactions among the chromophores, which is also considered in our model.

**Keywords:** Sol-gel films, chromophores, second harmonic generation, optical absorption, poling.

## 1. INTRODUCTION

Sol-gel materials exhibit some interesting features for linear and nonlinear optical applications<sup>1</sup>. Among the sol-gel method features it is remarkable the obtaining of highly homogeneous films starting from a liquid phase at room temperature. And it is also possible to incorporate optically active organic molecules (chromophores) to the material. In the sol-gel films the chromophores can maintain stable their optical properties better than in other kind of materials<sup>2</sup>.

Besides, the glassy transition temperature in sol-gel films can be higher than those ones of other polymeric materials. A high glassy transition temperature restrict the movement of the chromophores, thus the chromophores in sol-gel films can not be oriented as easy as in other materials, but the sol-gel films keep the chromophores orientation for a considerable long time at room temperature<sup>3</sup>.

Even more, sol-gel films can get crystalline structure by means of surfactant incorporation during the liquid phase stage of the sol-gel process<sup>4</sup>. All of these features becomes to the sol-gel films into a very interesting materials for diverse optical research and applications.

Chromophores with a high permanent dipole moment can be oriented toward a specific direction in a sol-gel film by means of the application of an intense external electric field<sup>5</sup>. The linear and nonlinear optical properties of these films depend on the application time of the external electric field (poling time). For example, both the optical absorption and the second harmonic generation of light by these kinds of films are different as the poling time increases.

Thus, it is important to understand and to describe the dynamical process involved in the chromophore orientation under the application of an external intense electric field, just like the corona one. There are some works about this topic, all of them do not provide a complete description of the physical process involved in the chromophores orientation as function of the poling time. The most representative descriptions for an applied DC field are those given by J. W. Wu<sup>6</sup> and by D. J. Binks et. al.<sup>7</sup>, and for an applied AC field are those given by Francesco Michelotti et. al.<sup>8</sup> and by Thomas G. Pedersen et. al.<sup>9</sup>

We are interested in the description of the chromophores orientation dynamics under the application of a DC field, but we are mainly interested in the existent descriptions lacks, due to the approximate nature of the descriptions. We propose a physical model which describes, also in an approximate way, the chromophore orientation dynamics, but paying attention to those aspects which were not taken into account by the previous works. These aspects are: a) the existence of a reasonable minimum value in the second order parameter (J. W. Wu<sup>6</sup> predicts the minimum but all its values are not physically acceptable, D. J. Binks et. al.<sup>7</sup> does not consider the minimum existence), b) the correct correspondence between the maximum value in the second order parameter and the asymptotic value given by the stationary rigid oriented gas model (ROGM)<sup>10</sup> (J. W. Wu<sup>6</sup> second order parameter maximum value does not correspond to the exact one given by the ROGM, D. J. Binks et. al.<sup>7</sup> second order parameter maximum value corresponds to the exact one given by the ROGM only for weak DC electric fields) and c) the incorporation of an effective electrostatic dipole-dipole interaction (J. W. Wu<sup>6</sup> and D. J. Binks et. al.<sup>7</sup> do not consider it).

In Section 2 the physical model is developed starting from a damped harmonic oscillator equation, in contrast to previous works which start from a rotational diffusion equation (RDE). In Section 3 we talk about the samples preparation and the experimental conditions under which the optical absorption and the second harmonic generation data were acquired. The experimental results, as well as their theoretical fits, are given in Section 4. Section 5 contains our conclusions.

## 2. THEORY

### 2.1 Optical absorption

The optical absorption  $\alpha$  of one chromophore with a double conjugated bonds system and with its main inertia moment  $I_{33}$  parallel to its main permanent dipole moment  $\mu_3^0$  can be written as

$$\alpha(\theta) = \alpha_m \sin^2 \theta, \quad (1)$$

where  $\alpha_m$  is the chromophore maximum optical absorption and  $\theta$  is the angle between the main chromophore axis and the direction of the incident light. Thus, the total absorbance  $A$  of a film with  $N$  chromophores can be written as

$$A = \alpha_0 \langle \sin^2 \theta \rangle, \quad (2)$$

with  $\alpha_0$  equal to  $N\alpha_m$  and “ $\langle \rangle$ ” the average over all the chromophores possible angles.

A dipolar chromophore under the influence of a DC electric field behaves like an oscillator. If we consider the chromophores oscillations as harmonic ones, the most general harmonic oscillator equation will describe the movement of each chromophore, i.e. each chromophore is described by the next equation

$$\ddot{\theta} + 2\gamma\dot{\theta} + \omega^2\theta = \frac{I_{33}E_d}{\mu_3^0}, \quad (3)$$

where each dot means a derivative with respect to poling time,  $\gamma$  means a damping constant (related to the matrix-chromophore interactions),  $E_d$  is an extra field related to the chromophore-chromophore electrostatic interaction, and  $\omega^2$  is the natural frequency oscillation given by

$$\omega = \sqrt{\frac{\mu_3^0 E}{I_{33}}}, \quad (4)$$

with  $E$  the local effective electrostatic field around the chromophores.

The most general solution to equation (3) for one chromophore is

$$\theta(t; \theta_0, \dot{\theta}_0) = \frac{F}{\omega^2} + \frac{\dot{\theta}_0 + \frac{(\theta_0\omega^2 - F)(\gamma + \Omega)}{\omega^2}}{2\Omega} e^{-(\gamma - \Omega)t} + \left( \theta_0 - \frac{F}{\omega^2} + \frac{-\dot{\theta}_0 + \frac{(F - \theta_0\omega^2)(\gamma + \Omega)}{\omega^2}}{2\Omega} \right) e^{-(\gamma + \Omega)t}, \quad (5)$$

with  $t$  the poling time,  $\theta_0$  the chromophore initial angle (before poling it can be any angle between 0 and  $2\pi$  with uniform probability),  $\dot{\theta}_0$  the chromophore initial angular speed,  $\Omega = \sqrt{\gamma^2 - \omega^2}$ , and  $F = \frac{I_{33} E_d}{\mu_3^0}$ .

Since the system has azimuthal symmetry the average of equation (2) can be calculated as

$$\left\langle \sin^2 \theta \left( t; \theta_0, \dot{\theta}_0 \right) \right\rangle_{\theta_0} = \frac{\int_{\theta_0=0}^{\theta_0=\pi} 2\pi \sin \theta_0 \sin^2 \theta \left( t; \theta_0, \dot{\theta}_0 \right) d\theta_0}{\int_{\theta_0=0}^{\theta_0=\pi} 2\pi \sin \theta_0 d\theta_0}, \quad (6)$$

with  $\theta \left( t; \theta_0, \dot{\theta}_0 \right)$  given by equation (5). The complete average is calculated by considering two most probable initial angular speeds, given by the chromophore thermal agitation

$$\dot{\theta}_0 = \pm \sqrt{\frac{k_B T}{I_{33}}}, \quad (7)$$

with  $k_B T$  all one chromophore thermal energy. Thus, the complete average is expressed as

$$\left\langle \sin^2 \theta \left( t; \theta_0, \dot{\theta}_0 \right) \right\rangle_{\theta_0, \dot{\theta}_0} = \frac{\left\langle \sin^2 \theta \left( t; \theta_0, +\dot{\theta}_0 \right) \right\rangle_{\theta_0} + \left\langle \sin^2 \theta \left( t; \theta_0, -\dot{\theta}_0 \right) \right\rangle_{\theta_0}}{2}, \quad (8)$$

being explicitly time dependent. As poling time increases equation (8) tends to zero, but that situation never occur in the real systems, due to the chromophores thermal agitation. Actually, the chromophores distributes around some central angle; the statistical distribution can be written as

$$G(\theta, t) = e^{\frac{\mu_3^0 E}{k_B T} \cos(\theta + \bar{\theta}(t))}, \quad (9)$$

with  $\bar{\theta}(t)$  the distribution central angle. For simplicity, we consider as the central angle to

$$\bar{\theta}(t) = \arcsin \left( \sqrt{\left\langle \sin^2 \theta \left( t; \theta_0, \dot{\theta}_0 \right) \right\rangle_{\theta_0, \dot{\theta}_0}} \right), \quad (10)$$

thus the useful average of equation (2) is

$$\left\langle \sin^2 \theta(t) \right\rangle = \frac{\int_{\theta=0}^{\theta=\pi} 2\pi \sin \theta [G(\theta, t) + G(-\theta, t)] \sin^2 \theta d\theta}{\int_{\theta=0}^{\theta=\pi} 2\pi \sin \theta [G(\theta, t) + G(-\theta, t)] d\theta}. \quad (11)$$

The optical absorption changes due to modifications in the chromophore orientation are usually expressed in terms of the second order parameter  $\Phi$ . The second order parameter has a straightforward relation to experimental data by the next equation

$$\Phi(t) = 1 - \frac{A(t)}{A(t=0)}. \quad (12)$$

In the other hand, the ROGM theoretically deduce the next second order parameter value for very large poling times, employing the statistical distribution of equation (9) centered at zero

$$\Phi = 1 + 3 \left( \frac{k_B T}{\mu_3^0 E} \right)^2 - \frac{3k_B T}{\mu E} \coth \left( \frac{\mu_3^0 E}{k_B T} \right). \quad (13)$$

Equations (12) and (13) are compatible, for very large poling times equation (10) tends to zero, in consequence, equation (9) becomes into the same statistical distribution considered by the ROGM. Thus, equation (12) contains the complete description of the material optical absorption as a function of the poling time.

In contrast, J. W. Wu<sup>6</sup> provides the next poling time dependent expression for the second order parameter

$$\Phi(t) = \frac{I_2 \left( \frac{\mu_3^0 E}{k_B T} \right)}{I_0 \left( \frac{\mu_3^0 E}{k_B T} \right)} \left( 1 - e^{-D_2 t} - \frac{3}{10} \frac{\mu_3^0 E}{k_B T} \frac{I_1 \left( \frac{\mu_3^0 E}{k_B T} \right)}{I_2 \left( \frac{\mu_3^0 E}{k_B T} \right)} (e^{-D_2 t} - e^{-D_3 t}) + \frac{1}{5} \frac{\mu_3^0 E}{k_B T} \frac{I_3 \left( \frac{\mu_3^0 E}{k_B T} \right)}{I_2 \left( \frac{\mu_3^0 E}{k_B T} \right)} (e^{-D_2 t} - e^{-D_3 t}) \right), \quad (14)$$

with  $D_n = n(n+1)D$ ,  $D$  a diffusion constant and  $I_n(x)$  the spherical modified Bessel functions. And D. J. Binks et. al.<sup>7</sup> propose their analogue expression for dispersive materials (the diffusion constant is also poling time dependent)

$$\Phi(t) = \Phi^\infty \left( 1 + \frac{\tau_1}{\tau_2 - \tau_1} t^{-\frac{1}{\tau_1}} - \frac{\tau_2}{\tau_2 - \tau_1} t^{-\frac{1}{\tau_2}} \right), \quad (15)$$

$$\text{with } \Phi^\infty = \frac{\left( \frac{\mu_3^0 E}{k_B T} \right)^2}{15 + \left( \frac{\mu_3^0 E}{k_B T} \right)^2} \text{ and } \tau_{1,2} = \left( 2D \left( 2 \mp \sqrt{1 - \frac{\left( \frac{\mu_3^0 E}{k_B T} \right)^2}{5}} \right) \right)^{-1}.$$

## 2.2 Second harmonic generation

The electric polarization of only one chromophore can be written as

$$p_i(t) = \mu_i^0 + \alpha_{ij} E_j(t) + \beta_{ijk} E_j(t) E_k(t) + \gamma_{ijkl} E_j(t) E_k(t) E_l(t) + \dots, \quad (16)$$

with  $p_i$  the microscopic polarization along the chromophore  $i$  axis,  $E_{j,k,l,\dots}$  the time dependent electric fields acting on the chromophore along the  $j, k, l, \dots$  chromophore axes,  $\alpha_{ij}$  the chromophore linear polarizability,  $\beta_{ijk}$  the chromophore second order hyperpolarizability and  $\gamma_{ijkl}$  the chromophore third order hyperpolarizability.

Besides, the macroscopic electric polarization for a chromophores system can be written as

$$P_I(t) = P_I^{(0)}(t) + \chi_{IJ}^{(1)}(t) E_J(t) + \chi_{IJK}^{(2)}(t) E_J(t) E_K(t) + \chi_{IJKL}^{(3)}(t) E_J(t) E_K(t) E_L(t) + \dots, \quad (17)$$

where  $P_I$  is the macroscopic polarization along the  $I$  laboratory axis,  $P_I^{(0)}$  is the system spontaneous polarization,  $\chi_{IJ}^{(1)}$  is the system first order susceptibility function,  $\chi_{IJK}^{(2)}$  is the system second order susceptibility function,  $\chi_{IJKL}^{(3)}$  is the system third order susceptibility function, and  $E_{J,K,L,\dots}$  are the electric fields acting on the chromophores system along the  $J, K, L, \dots$  laboratory axes.

The microscopic reference system axes are identified by numbers. The 3 axis is always along the main chromophore axis, and with the 1 and 2 axes form an orthogonal reference system. The orthogonal macroscopic reference system axes are identified by letters. The  $z$  and 3 axes give place to an angle  $\theta$  between them. And the 3 axis projection onto the  $x$ - $y$  plane forms an angle  $\phi$  with the  $x$  axis. This is just the relation between both reference systems.

The second order polarization of one chromophore with a double conjugated bonds system and with its main inertia moment  $I_{33}$  parallel to its main permanent dipole moment  $\mu_3^0$  can be written as

$$p_3^{(2)}(t) = \beta_{333} E_J(t) \cos(3, J)(t) E_K(t) \cos(3, K)(t). \quad (18)$$

And the chromophores system second order polarizations are

$$P_\eta^{(2)}(t) = N \int p_3^{(2)}(t) \sin(3, \eta)(t) G(\Omega) d\Omega, \quad (19)$$

with  $\eta = x, y, z$ ;  $N$  the chromophores number,  $G(\Omega)$  the chromophores statistical distribution and  $d\Omega$  a solid angle element. Thus, the nonzero second order susceptibility functions are  $\chi_{xx}^{(2)}(t) = \chi_{xy}^{(2)}(t) = \chi_{xz}^{(2)}(t) = \chi_{yz}^{(2)}(t)$ ,  $\chi_{yx}^{(2)}(t) = \chi_{zy}^{(2)}(t) = \chi_{zx}^{(2)}(t) = \chi_{xy}^{(2)}(t) = \chi_{xz}^{(2)}(t) = \chi_{yz}^{(2)}(t)$ ,  $\chi_{zz}^{(2)}(t)$ , which are explicitly expressed in the next equations

$$\begin{aligned} \chi_{xx}^{(2)}(t) &= N \int \beta_{333} \cos^2(3, x)(t) \cos(3, z)(t) G(\Omega) d\Omega = \\ &\frac{N}{2} \int \beta_{333} \sin^2(3, z)(t) \cos(3, z)(t) G(\Omega) d\Omega \end{aligned} \quad , \quad (20.1)$$

$$\begin{aligned} \chi_{yy}^{(2)}(t) &= N \int \beta_{333} \cos^2(3, y)(t) \cos(3, z)(t) G(\Omega) d\Omega = \\ &\frac{N}{2} \int \beta_{333} \sin^2(3, z)(t) \cos(3, z)(t) G(\Omega) d\Omega \end{aligned} \quad , \quad (20.2)$$

$$\begin{aligned} \chi_{zz}^{(2)}(t) &= N \int \beta_{333} \cos(3, z)(t) \cos^2(3, x)(t) G(\Omega) d\Omega = \\ &\frac{N}{2} \int \beta_{333} \cos(3, z)(t) \sin^2(3, z)(t) G(\Omega) d\Omega \end{aligned} \quad , \quad (20.3)$$

$$\chi_{zz}^{(2)}(t) = N \int \beta_{333} \cos^3(3, z)(t) G(\Omega) d\Omega \quad , \quad (20.4)$$

or equivalently

$$\chi_{xx}^{(2)}(t) = \chi_{xy}^{(2)}(t) = \chi_{xz}^{(2)}(t) = \chi_{yz}^{(2)}(t) = \frac{N\beta_{333}}{2} (\langle \cos \theta(t) \rangle - \langle \cos^3 \theta(t) \rangle), \quad (21.1)$$

$$\chi_{yy}^{(2)}(t) = \chi_{yx}^{(2)}(t) = \chi_{yz}^{(2)}(t) = \chi_{yx}^{(2)}(t) = \frac{N\beta_{333}}{2} (\langle \cos \theta(t) \rangle - \langle \cos^3 \theta(t) \rangle), \quad (21.2)$$

$$\chi_{zz}^{(2)}(t) = \chi_{zy}^{(2)}(t) = \chi_{zy}^{(2)}(t) = \chi_{zy}^{(2)}(t) = \frac{N\beta_{333}}{2} (\langle \cos \theta(t) \rangle - \langle \cos^3 \theta(t) \rangle), \quad (21.3)$$

$$\chi_{zz}^{(2)}(t) = N\beta_{333} \langle \cos^3 \theta(t) \rangle, \quad (21.4)$$

where “ $\langle \rangle$ ” are angular averages, which can be calculated following the same procedure explained in section 2.1.

By other side, the intensity of the illuminating beam of light  $I^\omega$ , the fundamental beam, can be expressed in terms of its electric field vectors as

$$I^\omega = \frac{c\epsilon_0\pi}{2} \langle |E_x^\omega(t)|^2 + |E_y^\omega(t)|^2 + |E_z^\omega(t)|^2 \rangle, \quad (22)$$

where  $\epsilon_0$  is the vacuum permittivity,  $c$  is the speed of light in vacuum and “ $\langle \rangle$ ” indicates a temporal average. Besides, for a non-polarized fundamental beam of light, its electric field magnitudes have the next values

$$|E_x^\omega| = \sqrt{\frac{I^\omega}{c\epsilon_0\pi}} \cos \xi, \quad (23.1)$$

$$|E_y^\omega| = \sqrt{\frac{I^\omega}{c\epsilon_0\pi}}, \quad (23.2)$$

$$|E_z^\omega| = \sqrt{\frac{I^\omega}{c\epsilon_0\pi}} \sin \xi, \quad (23.3)$$

with  $\xi$  the incident angle of the fundamental beam of light on the film surface. Figure 1 shows the geometrical relation among a chromophore, the light electric field vectors and an external DC electric field applied along the  $z$  axis.

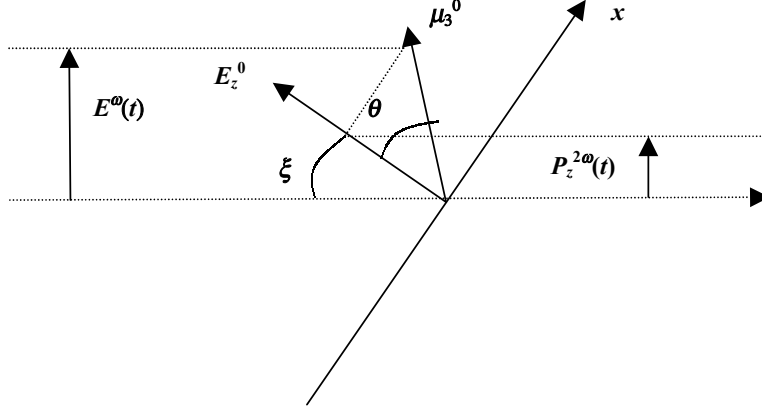


Fig. 1. Relation between microscopic and macroscopic coordinates. The fundamental beam and the second harmonic generated beam are shown.  $\theta$  is the angle between the chromophore main permanent dipolar moment and the external DC field along the  $z$  axis.  $\xi$  is the angle formed by the  $z$  axis and the fundamental beam of light direction. The  $x$  axis is on the incidence plane. The  $y$  axis is orthogonal to the incidence plane.  $E^\omega$  is any fundamental electric field component.  $P_z^{2\omega}$  is a polarization vector related to the harmonic electric field,  $P_z^{2\omega}$  is the chromophore induced polarization along the  $z$  axis.

Thus, the intensity of the second harmonic generated beam can be calculated in a similar way to equation (22)

$$I^{2\omega}(t) \propto \frac{c\epsilon_0\pi}{2} \left\langle |P_x^{(2)}(t)|^2 + |P_y^{(2)}(t)|^2 + |P_z^{(2)}(t)|^2 \right\rangle, \quad (24)$$

but with the macroscopic second order polarizations given, considering equations (19), (21) and (23), by

$$P_x^{(2)}(t) = \frac{N\beta_{333}I^\omega}{c\epsilon_0\pi} \left( \langle \cos\theta(t) \rangle - \langle \cos^3\theta(t) \rangle \right) (\cos\xi + 1) \sin\xi \cos\xi, \quad (25.1)$$

$$P_y^{(2)}(t) = \frac{N\beta_{333}I^\omega}{c\epsilon_0\pi} \left( \langle \cos\theta(t) \rangle - \langle \cos^3\theta(t) \rangle \right) (\cos\xi + 1) \sin\xi, \quad (25.2)$$

$$P_z^{(2)}(t) = \frac{N\beta_{333}I^\omega}{c\epsilon_0\pi} \left[ \langle \cos^3\theta(t) \rangle \sin^2\xi + \left( \langle \cos\theta(t) \rangle - \langle \cos^3\theta(t) \rangle \right) \left( \frac{1}{2} + \cos\xi + \frac{\cos^2\xi}{2} \right) \right] \sin\xi. \quad (25.3)$$

From equations (24) and (25) it is possible to obtain an expression for the SHG intensity as function of the poling time

$$\frac{I^{2\omega}(t)}{(N\beta_{333}I^\omega)^2 \sin^2\xi} \propto \left( \left( \langle \cos\theta(t) \rangle - \langle \cos^3\theta(t) \rangle \right)^2 (\cos\xi + 1)^2 (\cos^2\xi + 1) + \left( \langle \cos^3\theta(t) \rangle \sin^2\xi + \left( \langle \cos\theta(t) \rangle - \langle \cos^3\theta(t) \rangle \right) \left( \frac{1}{2} + \cos\xi + \frac{\cos^2\xi}{2} \right) \right)^2 \right), \quad (26)$$

where the angular averages can be calculated as was done in section 2.1.

J. W. Wu<sup>6</sup> employs the next equations for the angular averages evaluation

$$\langle \cos \theta(t) \rangle - \langle \cos^3 \theta(t) \rangle = \frac{2}{5} \left( \frac{I_1 \left( \frac{\mu_3^0 E}{k_B T} \right)}{I_0 \left( \frac{\mu_3^0 E}{k_B T} \right)} \left( 1 - e^{-2Dt} + \frac{1}{6} \frac{\mu_3^0 E}{k_B T} I_2 \left( \frac{\mu_3^0 E}{k_B T} \right) (e^{-2Dt} - e^{-6Dt}) \right) - \frac{I_3 \left( \frac{\mu_3^0 E}{k_B T} \right)}{I_0 \left( \frac{\mu_3^0 E}{k_B T} \right)} \left( 1 - e^{-12Dt} - \frac{2}{7} \frac{\mu_3^0 E}{k_B T} I_2 \left( \frac{\mu_3^0 E}{k_B T} \right) (e^{-6Dt} - e^{-12Dt}) \right) + \frac{3}{14} \frac{\mu_3^0 E}{k_B T} I_4 \left( \frac{\mu_3^0 E}{k_B T} \right) (e^{-12Dt} - e^{-20Dt}) \right), \quad (27.1)$$

$$\langle \cos^3 \theta(t) \rangle = \frac{3}{5} \frac{I_1 \left( \frac{\mu_3^0 E}{k_B T} \right)}{I_0 \left( \frac{\mu_3^0 E}{k_B T} \right)} \left( 1 - e^{-2Dt} + \frac{1}{6} \frac{\mu_3^0 E}{k_B T} I_2 \left( \frac{\mu_3^0 E}{k_B T} \right) (e^{-2Dt} - e^{-6Dt}) \right) + \frac{2}{5} \frac{I_3 \left( \frac{\mu_3^0 E}{k_B T} \right)}{I_0 \left( \frac{\mu_3^0 E}{k_B T} \right)} \left( 1 - e^{-12Dt} - \frac{2}{7} \frac{\mu_3^0 E}{k_B T} I_2 \left( \frac{\mu_3^0 E}{k_B T} \right) (e^{-6Dt} - e^{-12Dt}) \right) + \frac{3}{14} \frac{\mu_3^0 E}{k_B T} I_4 \left( \frac{\mu_3^0 E}{k_B T} \right) (e^{-12Dt} - e^{-20Dt}). \quad (27.2)$$

D. J. Binks et. al.<sup>7</sup> propose the next equations for the angular averages evaluation

$$\langle \cos \theta(t) \rangle - \langle \cos^3 \theta(t) \rangle = \frac{2 \frac{\mu_3^0 E}{k_B T}}{15 + \left( \frac{\mu_3^0 E}{k_B T} \right)^2} \left( 1 + \frac{\tau_1}{\tau_2 - \tau_1} t^{-\frac{1}{\tau_1}} - \frac{\tau_2}{\tau_2 - \tau_1} t^{-\frac{1}{\tau_2}} \right) - \frac{4}{15} D \frac{\mu_3^0 E}{k_B T} \frac{\tau_1 \tau_2}{\tau_2 - \tau_1} \left( t^{-\frac{1}{\tau_1}} - t^{-\frac{1}{\tau_2}} \right), \quad (28.1)$$

$$\langle \cos^3 \theta(t) \rangle = \frac{3 \frac{\mu_3^0 E}{k_B T}}{15 + \left( \frac{\mu_3^0 E}{k_B T} \right)^2} \left( 1 + \frac{\tau_1}{\tau_2 - \tau_1} t^{-\frac{1}{\tau_1}} - \frac{\tau_2}{\tau_2 - \tau_1} t^{-\frac{1}{\tau_2}} \right) - \frac{2}{5} D \frac{\mu_3^0 E}{k_B T} \frac{\tau_1 \tau_2}{\tau_2 - \tau_1} \left( t^{\frac{1}{\tau_1}} - t^{\frac{1}{\tau_2}} \right) \quad (28.2)$$

### 3. EXPERIMENTAL

All the studied samples were SiO<sub>2</sub> films prepared by the sol-gel process. All of the films were doped with the nonlinear chromophore Disperse Red 1 (DR1), because this chromophore possesses an important permanent dipolar moment ( $\mu_3^0 = 8.7 \text{ D}^1$ ).

Two kinds of samples were employed for the optical absorption studies: amorphous and nanostructured. Two amorphous films were prepared by spin-coating with the DR1 chromophores linked to the SiO<sub>2</sub> matrix, these films differ themselves in the presence of Carbazole, one of them does not contain Carbazole molecules.<sup>11,12</sup> In the other hand, four nanostructured samples were prepared by dip-coating with the DR1 chromophores as guests, these films differ themselves in their crystalline structure: lamellar, hexagonal or mixed; for one of the lamellar samples it was employed the ionic surfactant Sodium Dodecyl Sulfate (SDS)<sup>13</sup>, the rest of the samples were prepared with different molar ratios between Carbazole and the ionic surfactant Cetyl Trimethyl Ammonium Bromide (CTAB)<sup>4</sup>. The studied nanostructured samples exhibit one of the X-ray spectra shown in figure 2.

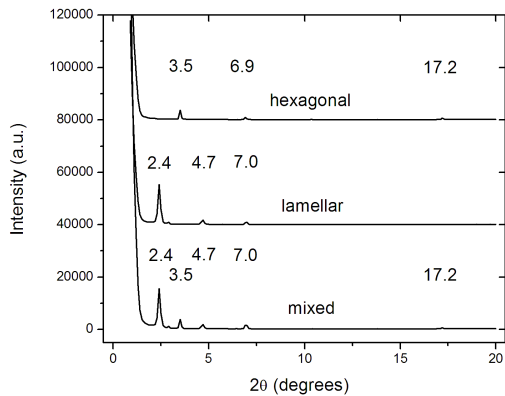


Fig. 2. X-ray diffraction patterns obtained for each one of the nanostructured films. Mixed crystalline order share the lamellar and hexagonal X-ray diffraction peaks.

For the SHG studies all the samples were amorphous. These samples were prepared by spin-coating with the DR1 chromophores linked to the SiO<sub>2</sub> matrix in the next DR1:Carbazole:TEOS molar ratios: 1:3:1, 1:5:1, 1:10:1 and 1:20:1.<sup>11</sup> The chromophores orientation was induced by means of the usual single point corona technique<sup>5</sup>, employing a DC voltage equal to 6 KV, an electrodes separation distance equal to 12 mm and a poling temperature equal to 120°C. The optical absorption studies were carried out with a ThermoSpectronic Genesys 2 spectrophotometer. The optical absorption was recorded for different samples poling times, employing a 490 nm wavelength natural light at normal incidence (incident light reached the film with the same applied corona field direction). The SHG studies were carried out in-situ during the corona poling. The fundamental beam of light was provided by a non-polarized Nanolase YAG:Nd laser at 1064 nm, the SHG intensity detector was a Hamamatsu photomultiplier and the data acquisition was carried out by a Tektronix oscilloscope. Figure 3 shows an experimental setup schematic diagram.

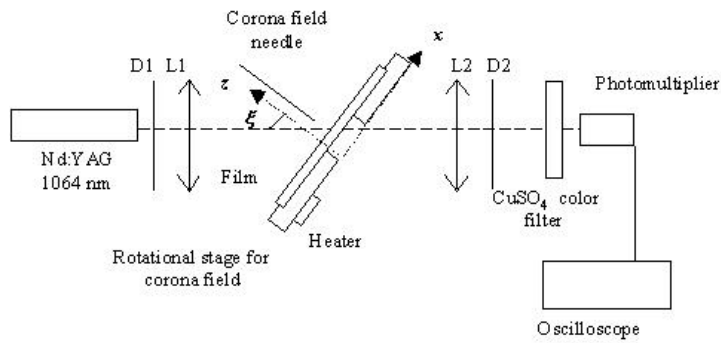


Fig. 3. SHG experimental setup. Horizontal dotted line represents the system optical axis. D1 and D2 are diaphragms. L1 and L2 are positive lenses. The color filter absorbs the fundamental beam of light but allows to the SHG beam to reach the photomultiplier. And the  $\xi$  angle was the same for all the studied films ( $80^\circ$ ).

#### 4. RESULTS

The optical absorption experimental results as well as their theoretical fits are shown in figures 4 and 5. The fitting parameters are shown in table 1. The fits corresponding to our model were done following the reported procedure<sup>14</sup>. The fits corresponding to the J. W. Wu model were done employing equation (14). In figure 5a) there are two J. W. Wu model fits, one of them is consistent with the maximum order parameter  $\Phi_{\max}$ , the other one with the minimum  $\Phi$ .

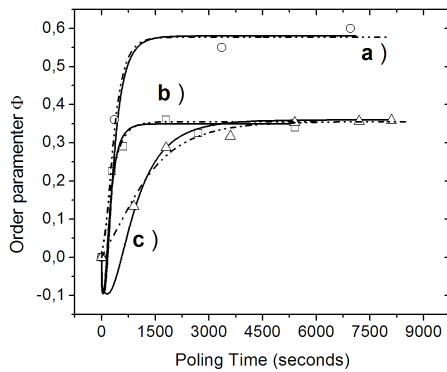


Fig. 4. Optical absorption experimental results with their corresponding fits for: a) lamellar film with SDS, b) amorphous film with Carbazole and c) amorphous film without Carbazole. Symbols represent experimental data. Continuous lines are our model fits. Dotted lines are the J. W. Wu model fits.

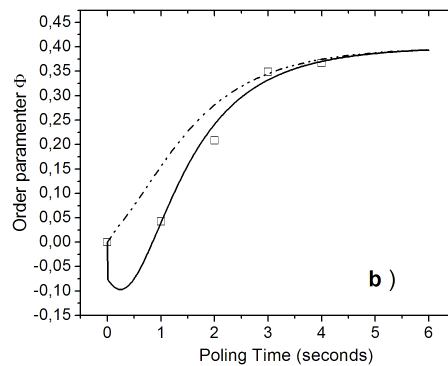
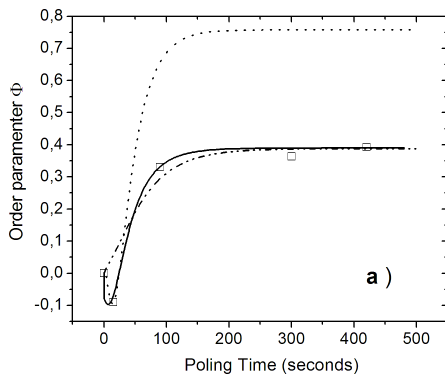


Fig. 5. a) Optical absorption experimental results with their corresponding fits for a lamellar film with CTAB. b) Optical absorption experimental results with their corresponding fits for a hexagonal film with CTAB. Symbols represent experimental data. Continuous lines are our model fits. Dotted lines are the J. W. Wu model fits.

Our optical absorption experimental data can not be fitted by the D. J. Binks et. al. model, because our order parameters are out of the D. J. Binks et. al. model validity region. The optical experimental data of the sample with a mixed nanostructure do not appear in figures 4 and 5, because the sample exhibited optical degradation, however the sample shown a minimum in the second order parameter  $\Phi$ .

Table 1. Fitting parameters employed in figures 4 and 5. There are two values for some fitting parameters of the Lamellar (CTAB) sample, they correspond to the couple of J. W. Wu model fits shown in figure 5a).

Sample	$\gamma$ (s <sup>-1</sup> )	$\Phi_{\max}$	$D_{Wu}$ (s <sup>-1</sup> )	$(\mu_3^0 E/k_B T)_{Wu}$
Lamellar (SDS)	$7.0 \times 10^{24}$	0.58	0.00200	4.10
Amorphous with Carbazole	$2.5 \times 10^{24}$	0.35	0.00200	2.30
Amorphous without Carbazole	$1.0 \times 10^{25}$	0.36	0.00048	2.30
Lamellar (CTAB)	$5.0 \times 10^{23}$	0.39	0.01000 (0.02200)	2.50 (7.70)
Hexagonal (CTAB)	$1.8 \times 10^{22}$	0.39	0.40000	2.57

The SHG intensity experimental results as well as their theoretical fits are shown in figure 6. The fitting parameters are shown in table 2. The fits corresponding to our model were done following the reported procedure<sup>15</sup>. The fits corresponding to the J. W. Wu model were done employing equations (27). The fits corresponding to the D. J. Binks et. al. model were done employing equations (28).

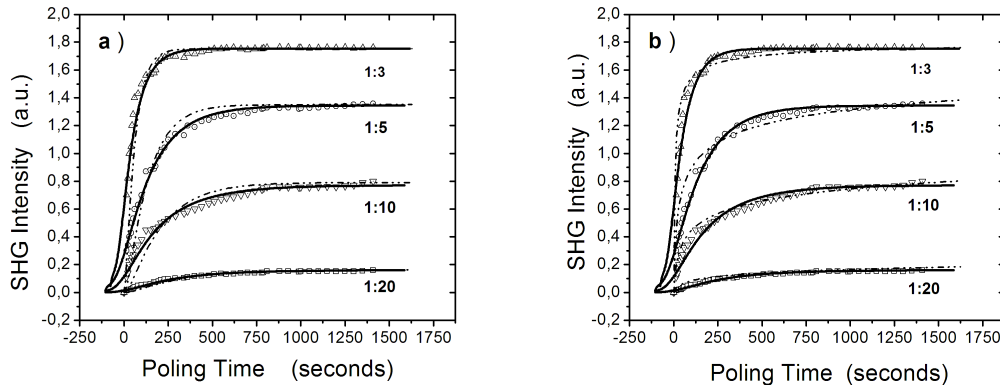


Fig. 6. SHG intensity experimental results with their corresponding fits. Symbols represent the experimental data. a) Continuous lines are our model fits, dotted lines are the J. W. Wu model fits. b) Continuous lines are our model fits, dotted lines are the D. J. Binks et. al. model fits.

Table 2. Fitting parameters employed in figure 6.  $C$  is proportional to  $(N\beta_{333}I^{0})^2$  and  $T_s$  is a time shift. It was considered a  $\mu_3^0 E/k_B T$  value equal to 3.1, consistent with experimental data, for our model and for the J. W. Wu one. For the D. J. Binks et. al. model, a  $\mu_3^0 E/k_B T$  value in its validity region was considered: 1.0.

	$\gamma$ (s <sup>-1</sup> )	$C$ (a.u.)	$T_s$ (s)	$E_d$ (V/m)	$D_{Wu}$ (s <sup>-1</sup> )	$C_{Wu}$ (a.u.)	$D_{Binks}$ (s <sup>-1</sup> )	$C_{Binks}$ (a.u.)
1:20	$0.45 \times 10^{25}$	0.38	110	0	0.0018	0.28	0.030	14
1:10	$0.34 \times 10^{25}$	1.84	110	0	0.0028	1.34	0.071	19
1:5	$0.22 \times 10^{25}$	6.08	110	$3.999 \times 10^8$	0.0044	2.29	0.110	22
1:3	$0.11 \times 10^{25}$	17.06	80	$6.056 \times 10^8$	0.0099	2.97	0.250	20

In figures 4, 5 and 6 our model exhibits a good agreement with experimental data. In figure 4 our model follows the same behavior than the J. W. Wu one at large poling times, but there are differences between them at short poling times, it is most evident from figures 4c), 5a) and 5b). In figure 5a) our model agrees with all the experimental data, but J. W. Wu model is not able to fit both short poling and long poling times experimental data. Table 1 show an inverse but consistent behavior between the damping constant  $\gamma$  and the diffusion one  $D$ , both are related to the chromophores mobility but their experimental order of magnitude are quite different. With the  $\Phi_{\max}$  knowledge, both models require of only one material parameter.

There are some details to consider in figures 6. Our model fits experimental data very well, but with a shifted plot, maybe due to the model harmonicity assumption. J. W. Wu and D. J. Binks et. al. models immersed in equation (26) follow in a qualitative way the experimental data behavior, but they do not obtain an exact match between experimental data and the model. In figure 6b) the dotted line does not take an asymptotic behavior, the dotted line raise continuously as the poling time increases, which means that our materials are not dispersive (in the D. J. Binks et. al. model sense), being better described by the other two models. In table 2, the  $C$  parameter of our model is in a good agreement with the samples molar ratios, due to the incorporation of an effective dipole-dipole electrostatic interaction; the  $C$  parameter of the J. W. Wu model increases with the chromophores concentration but not as expected, and the D. J. Binks model does not follow the same pattern than the other two models. With respect to the chromophores mobility parameters  $\gamma$  and  $D$  of table 2, all of them are consistent.

## 5. CONCLUSIONS

It was proposed a physical model for the chromophores orientation dynamics, in amorphous and nanostructured sol-gel films, under the presence of a corona field. The orientation was studied experimentally with optical absorption and SHG intensity measurements in the films for different poling times. The experimental results were satisfactorily fitted by our model. For comparison, other two models fitted the experimental data. From one of them we can say that our samples were not dispersive. The incorporation of the dipole-dipole electrostatic interactions in our model had not been considered by the other two, being this interaction the one which explain some features of the SHG experimental data behavior.

## ACKNOWLEDGMENTS

This work has been supported by the following grants: CONACYT 43226-F, NSF-CONACYT, ECOS M02-P02, and PAPIIT 116506-3.

## REFERENCES

1. Frederic Chaumel, Hongwei Jiang, and Ashok Kakkar. "Sol-Gel Materials for Second-Order Nonlinear Optics", *Chem. Mater.* 13, 3389-3395, 2001.
2. A. Costela, I. García-Moreno and R. Sastre. "Polymeric solid-state dye lasers: Recent developments", *Phys. Chem. Chem. Phys.* 5, 4745-4763, 2003.
3. Hélène Goudket, Michael Canva, and Yves Lévy, Frédéric Chaput and Jean-Pierre Boilot. "Temperature dependence of second-order nonlinear relaxation of a doped chromophore-doped sol-gel material", *J. Appl. Phys.* 90, 6044-6047, 2001.
4. J. A. García M., Guadalupe Valverde, and Jeffrey I. Zink. "Using Carbazole as a Structural Modifier of CTAB-Templated Silicate Sol-Gel Thin Films", *Langmuir.* 19, 4411-4414, 2003.
5. M. A. Mortazavi, A. Knoesen, and S. T. Kowel, B. G. Higgins, A. Dienes. "Second-harmonic generation and absorption studies of polymer-dye films oriented by corona-onset poling at elevated temperatures", *J. Opt. Soc. Am. B* 6, 733-741, 1989.
6. J. W. Wu. "Birefringent and electro-optic effects in poled polymer films: steady-state and transient properties", *J. Opt. Soc. Am. B* 8, 142-152, 1991.
7. D. J. Binks, K. Khand and D. P. West. "Poling and relaxation of dipoles in dispersive media", *J. Appl. Phys.* 89, 231-236, 2001.
8. Francesco Michelotti, Eric Toussare. "Pulse poling of side-chain and crosslinkable copolymers", *J. Appl. Phys.* 82, 5726-5744, 1997.
9. Thomas G. Pedersen, Kim Jespersen and Per M. Johansen, John Wyller. "dc and ac Electro-optic response of chromophores in a viscoelastic polymer matrix: analytical model", *J. Opt. Soc. Am. B* 19, 2622-2631, 2002.
10. R. H. Page, M. C. Jurich, B. Reck, A. Sen, R. J. Twieg, J. D. Swalen, G. C. Bjorklund, and C. G. Wilson. "Electrochromic and optical waveguide studies of corona-poled electro-optic polymer films", *J. Opt. Soc. Am. B* 7, 1239-1250, 1990.
11. J. A. Reyes-Esqueda, B. Darracq, J. García-Macedo, M. Canva, M. Blanchard-Desce, F. Chaput, K. Lahlil, J. P. Boilot, A. Brun, Y. Lévy. "Effect of chromophore-chromophore electrostatic interactions in the NLO response of functionalized organic-inorganic sol-gel materials", *Opt. Comm.* 198, 207-215, 2001.
12. Po-Hou Sung, Shao-Ling Wu, Chien-Yang Lin. "Sol-gel process of non-linear optical silica films with organic chromophore as side chain" *J. Mater. Sci.* 31, 2443-2446, 1996.

13. G. Valverde, J. García-Macedo, D. Cruz, J. I. Zink, R. Hernández. "Photoconductivity in Mesostructured Thin Films", *J. Sol-Gel Sci. & Tech.* 26, 605-608, 2003.
14. Alfredo Franco, Guadalupe Valverde-Aguilar and Jorge García-Macedo. "Orientational dynamics of DR1 molecules in sol-gel films", *Opt. Mat.* In press.
15. Alfredo Franco, Guadalupe Valverde-Aguilar, Jorge García-Macedo, Frederic Chaput, Michael Canva and Yves Levy. "Modeling of the second harmonic generation in SiO<sub>2</sub> sol-gel films doped with nanoscopic DR1 molecules as function of the poling time", *Opt. Mat.* In press.